Available online at www.sciencedirect.com

ScienceDirect

Proceedings of the Combustion Institute 37 (2019) 5499–5506

Proceedings of the Combustion Institute

www.elsevier.com/locate/proci

Flame spray pyrolysis synthesized CuO-TiO_2 nanoparticles for catalytic combustion of lean CO

Xin Chen, Zuwei Xu*, Fan Yang, Haibo Zhao*

State Key Laboratory of Coal Combustion, Huazhong University of Science and Technology Wuhan 430074, PR China

Received 1 December 2017; accepted 26 May 2018
Available online 12 June 2018

Abstract

In this work, CuO-TiO_2 nanoparticles with different CuO mass contents of 2%, 8%, 12%, and 20% are synthesized by flame spray pyrolysis (FSP) method and applied to catalytic combustion of lean CO. The nano-catalyst is characterized by N_2-physisorption isotherms, X-ray diffraction (XRD), transmission electron microscopy (TEM), H_2-TPR (temperature-programmed reduction) and X-ray photoelectron spectroscopy (XPS). All the catalysts possess a high specific surface area, of which the CuO-TiO_2 nanoparticles with 2 wt.% Cu (2CT) is as high as 98 m^2/g, and exhibits a spherical structure with a diameter of 15–20 nm. Compared with other methods, the FSP method can significantly improve the loading of CuO without producing large crystalline CuO particles on the catalyst surface. Interestingly, the addition of CuO will essentially change the lattice structure of TiO_2 for all catalysts, including its crystal spacing and XRD diffraction angle. Copper cations are embedded in TiO_2 lattice to promote the transformation from anatase to rutile by producing oxygen defect at high flame temperature. The interaction between CuO and TiO_2 has significant influence on its physicochemical properties. A lower onset reduction temperature on the sample with higher CuO loading is obtained due to the hydrogen spillover effect in H_2-TPR test. Moreover, the loaded CuO increases the content of more stable rutile phase in the materials, so that it reduces the strong metal-support interaction (SMSI) effect of CuO and anatase phase to improve the properties of CO catalytic combustion. The synthesized CuO-TiO_2 nanoparticles can achieve complete combustion conversion of lean CO at lower temperature of 120°C.

Keywords: Flame spray pyrolysis; CuO-TiO_2 catalysts; CO catalytic combustion; Phase transformation; Support-metal oxide interaction

1. Introduction

Removal of lean CO is becoming increasingly important in a variety of industry processes, such as cleaning exhaust gas, lowering automotive emissions, and exhaust abatement in breathing apparatus [1]. Low-temperature catalytic oxidation of lean CO has attracted a growing interest of scientific and industrial communities because it can provide an economic and efficient CO clean-up technique. For catalytic combustion applications, supported noble metal catalysts exhibit high

* Corresponding authors.
E-mail addresses: xuzw@hust.edu.cn (Z. Xu), hzhao@mail.hust.edu.cn (H. Zhao).

https://doi.org/10.1016/j.proci.2018.05.102
1540-7489

reaction activity and stability [2]. Considering the limited resources and high cost of noble metals, the development of earth-abundant, cheap and efficient catalysts is of particular importance. Copper-based catalysts have been found to be an excellent candidate due to its relatively high catalytic performance and low cost [2]. However, pure copper-based catalyst is less active and stable than the noble metal catalysts [3]. Introducing different supports into the catalysts system is an effective way to improve the reactivity and stability of Cu based catalysts [4]. CeO_2, TiO_2, Al_2O_3, MgO and ZrO_2 are the more common supports. Among them, TiO_2 shows a favorable effect on the activity of the catalysts due to its outstanding oxygen storage capacity (OSC) [5]. Furthermore, owing to the strong metal-support interaction (SMSI) effect, the metal oxide supported on TiO_2 can obtain better stability and dispersion [6].

The CuO-TiO_2 catalysts have been prepared in a variety of ways, such as impregnation, sol-gel and hydrothermal methods [7,8]. In the CuO-TiO_2 composite nanomaterials, CuO species of high dispersion, e.g., isolated ions and smaller crystalline, have higher reactivity than larger crystalline CuO and play a major role in CO catalytic combustion [9]. However, when the content of CuO exceeds a certain value, large grains of CuO are often appearing in these preparation methods, which is considered to be responsible for the decline of the material performance. For different preparation methods, the threshold value of CuO content is different. For instance, the value is about 5–10% for impregnation method, and 8–12% for sol-gel method [10]. Since low CuO loading results in a decrease of the active phase content, increasing the content of CuO in the system without the formation of large crystalline CuO species is vital to high-performance CuO-TiO_2 nano-catalysts.

Flame spray pyrolysis (FSP) is a fast and economical route to produce nanoparticles with homogeneous morphology and narrow size distribution. Compared with other methods, the most attractive advantage of FSP is the ability to handle a very wide range of precursor types and one-step synthesize ultrafine particles. The prepared materials demonstrate high purity, good dispersion, controllable structure and composition [11]. Numerous high performance nano-catalysts have been prepared by FSP synthesis, which prove that the synthesis method is a very attractive preparation route for nanocomposites [12–14]. During the FSP synthesis process, the composite material can be mixed at the atomic level. In addition, the copper ions in the material will not spillover to the surface because the calcination process, which may lead to a greater instability of the crystal structure of TiO_2. is not needed [15,16]. Although the FSP-synthesized nanocomposites have been successfully applied to many science and engineering fields, to the best of our knowledge, no open publication is related to catalytic combustion of lean CO over the FSP-made CuO-TiO_2 nanoparticles.

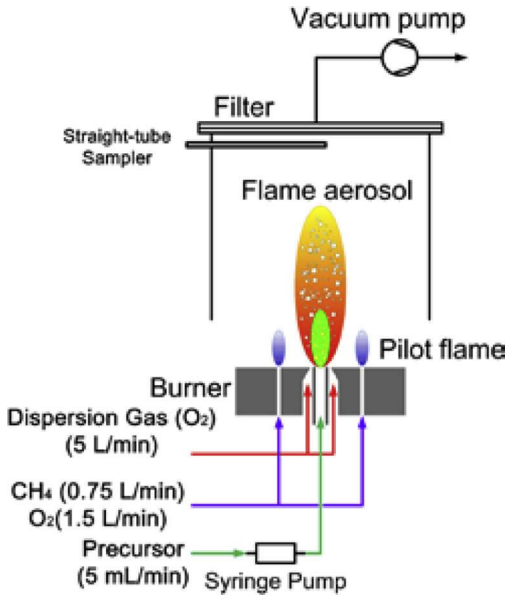

Fig. 1. Flame Spray Pyrolysis System schematic of the experimental.

Here we report the FSP synthesis of CuO-TiO_2 nanocomposite with different Cu loading, their physiochemical characterization and catalytic performance for low-temperature oxidation of lean CO. The morphology and phase composition of catalysts are characterized by Brunauer–Emmett–Teller method (BET), X-ray diffraction (XRD), Transmission electron microscopy (TEM), X-ray photoelectron spectroscopy (XPS), and H_2-temperature programmed reduction (H_2-TPR). The effects of the content of CuO on the structure, morphology and chemical properties of the CuO-TiO_2 composite are carefully examined as thus rational mechanisms of reactivity are proposed.

2. Experimental

2.1. Catalyst preparation

The CuO-TiO_2 catalysts are synthesized in a commercial laboratory-scale FSP system (NPS10, Tethis SpA). As shown in Fig. 1, the mixed solution of precursor and liquid fuel is injected by a syringe pump into an external-mixing atomizing nozzle that is made of a capillary tube, and the solution is dispersed into fine droplets by the coaxial dispersion gas flow. A premixed methane-oxygen pilot flame ignites the atomized precursor solution resulting in the formation of a high-temperature flame within which the organometallic precursors decompose and the organic compounds undergo

complete combustion. The metallic components of the precursor will then nucleate and condensate to form primary particles of oxides. Aggregation will take place in the high temperature region of the flame followed by rapid quenching due to intensive convection. Thus the primary particles will remain small though they do form loose agglomerates in the aerosol stream [17]. In the strong turbulent high temperature flame, the precursor will be torn to atoms or ions, resulting in a high degree of mixing which ensures good dispersion and makes it possible to enhance the efficient loading in materials.

The aerosol downstream is extracted and rapidly diluted by a straight-tube sampler and connected with a scanning mobility particle sizer (SMPS, Model 3938, TSI, USA), and the particle size distribution functions (PSDs) of the synthesized particles are measured by the SMPS. The powders are collected on a glass microfiber filter with the aid of a vacuum pump, located above the FSP burner. Detailed preparation of precursor solution and the parameters of FSP synthesis are shown in **Section S1**, Supplemental Materials (SM).

2.2. Catalyst characterization

Nitrogen sorption isotherms at −196°C are measured using a physisorption apparatus (Micromeritics ASAP 2020, USA). The specific surface area (SSA) is calculated using the Brunauer–Emmett–Teller (BET) method. XRD patterns are obtained with a RU-200B diffractometer (Rigaku, Japan) using Cu Kα radiation ($\lambda = 1.5406$ Å). The morphology and crystalline phase of the particles is analyzed with a TEM (JEOL 2100F, Japan) with an acceleration voltage of 200 kV. XPS analysis is performed on a high performance electron spectrometer (Thermo ESCALAB 250, Thermo Fisher, USA), using Al Kα radiation (1486.6 eV) operating at an accelerating power of 150 W. All binding energies (BEs) are referenced to the adventitious C 1 s at 284.6 eV. H_2-TPR is carried out on an automated Micromeritics AutoChem II-2920 instrument (Micromeritics, USA). For H_2-TPR analysis, 100 mg of sample is heated in N_2 (50 mL /min) from room temperature to 150°C and held for 1 h, subsequently cooled to room temperature in a N_2 atmosphere and switched to the stream of 10 vol% H_2/Ar (50 mL/min) and held for 20 min. Then the sample is heated from room temperature to 300°C in H_2 at a heating rate of 10°C/min.

2.3. Catalytic activity test

The catalytic combustion of CO to CO_2 over the as-prepared CuO-TiO_2 nano-catalysts is conducted in a fixed-bed quartz tube reactor (i.d = 8 mm). The sample of each catalyst is loaded in the reactor and pretreated for 1 h by passing N_2 gas (100 mL/min) through the catalysts heated at 120°C to completely dry and remove adsorbed surface species. A feed stream of 1.5 vol% CO, 6 vol% O_2, and 93 vol% N_2 as diluent is introduced into the reactor at a space velocity (SV) of 60,000 mL/(g·h). Online analysis of effluent gas is measured using a gas chromatograph (Synpec 3000B, China) equipped with a thermal conductivity detector (TCD). The reactor and detailed experimental procedures are also presented in **Section S2**, SM. The conversion rate of CO is calculated by subtracting the CO outlet concentration from the CO inlet concentration and dividing by the inlet concentration. The kinetic parameters of CO catalytic combustion are calculated (see **Section S3** of SM for more details).

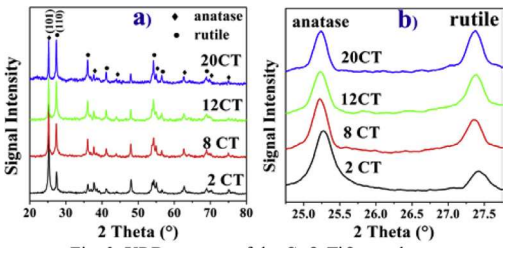

Fig. 2. XRD patterns of the CuO-TiO_2 catalysts.

3. Results and Discussion

3.1. Catalysts structural characterization

Table 1 provides the BET specific surface area (SSA) of the catalysts and their BET equivalent diameter. Noted that the SSA of the catalysts present a decrease from 98.96 m^2/g (2CT) to 70.07 m^2/g (20CT) with the increase of CuO content. As shown in Fig. 2b, the diffraction peaks of anatase ($2\theta = 25.3°$, [PDF-ICDD 21-1272]) and rutile ($2\theta = 27.4°$, [PDF-ICDD 21-1276]) become narrower with the addition of CuO, suggesting that the crystallite size of both anatase and rutile increase when increasing CuO content, which is consistent with the change trend of BET equivalent diameter and the SMPS results (see Fig. S3 in **Section S4**, SM). As seen, the intensity of the main rutile reflection increases, which indicates an increased rutile phase resulting from the transformation of anatase to rutile. The mass fraction of rutile phase increases from 27.6 wt.% of 2CT to 56.2 wt.% of 12CT. However, rutile phase increases slightly when CuO content increases from 12 wt.% to 20 wt.%. The phenomenon that the addition of transition-metal dopants increase the crystallite sizes of TiO_2 and resulting in larger crystallite size during particle formation in the high-temperature flame has also been reported in other literatures [16,18]. The copper cations with the valence state less than the valence of Ti^{4+} and a small ionic radius can sub-

Table 1
XRD and BET data for the CuO-TiO_2 catalysts.

Catalysts	CuO content [a]	BET surface area (m^2/g)	BET equivalent diameter [b]	Anatase (wt.%)[c]	Rutile (wt.%)[c]
2CT	2%	98.96	15.0	72.3	27.6
8CT	8%	83.56	18.0	51.0	49.0
12CT	12%	77.28	19.4	43.8	56.2
20CT	20%	70.07	21.4	43.1	56.9

[a] Calculated by the equation: $CuO\ wt\% = m_{CuO}/(m_{CuO}+m_{TiO_2}) \times 100\%$, where m_{CuO} and m_{TiO_2} are the mass of CuO and TiO_2 in the material, respectively.
[b] the particle size was calculated by the formula: $d_{BET} = 6/(S_a \times \rho)$, where S_a is the BET surface area, ρ is the density of particle.
[c] Calculated by the equation: $W_{Rutile} = (1 + 0.8^* I_A/I_R)^{-1}$, where I_A and I_R are the relative intensity of the main diffraction peaks of anatase and rutile, respectively [21].

stitutionary enter the TiO_2 lattice and promote the formation of oxygen vacancies by reduction of dopant Cu^{2+} [19]. The presence of oxygen vacancies enhances the diffusion of oxygen ions. As a result, the TiO_2 sintering rate controlled by the diffusion of oxygen ions will increase. Furthermore, the second Ti_nO_{2n-1} intermediates due to the formation of oxygen vacancy are the nucleation center for rutile, which accelerates the transformation of anatase to rutile [20].

The evidence of the embedding of copper cations into the TiO_2 lattice is also found in XRD and TEM results. The diffraction angle of the catalysts shows a slight shift with the change of Cu contents, which indicates that the copper cations embed into the TiO_2 lattice to form solid solution and thus affect the crystal structure of TiO_2 [22]. Direct measurement of the lattice spacing of the (110) plane of rutile and the (101) plane of anatase gives the value of 0.324 nm and 0.356 nm, respectively. There is a little deviation between the crystalline interplanar space and the standard distance, which is also attributed to the effect of doped copper cations.

No CuO/Cu_2O/Cu peak is detected in the CuO-TiO_2 diffraction patterns even at the highest CuO content of 20 wt.%. This could be attributed to highly-dispersed Cu species which are too small to be detectable by XRD. As shown in Fig. 3, the TEM micrographs and SAED (selected area electron diffraction) images of the catalysts also confirm this phenomenon. The catalysts exhibit spherical morphology with a uniform particle size distribution and a mean particle size of ~20 nm, which agrees with BET equivalent diameter. Only dispersed CuO clusters with a diameter less than 4 nm are found in SAED and TEM images of 20CT. No small crystals of CuO or Cu_2O are found in these catalysts. Meanwhile, there is a layer of material without crystal structure at the edge of the particle, which could be amorphous CuO or Cu_2O species. Thus, highly dispersed CuO species are successfully formed on the TiO_2 particles [5]. For the catalyst prepared by other methods, only when the content of CuO is below 12 wt.%, there were no large particles observed on the surface of TiO_2. The above results show that the FSP method almost doubles the threshold value of CuO content.

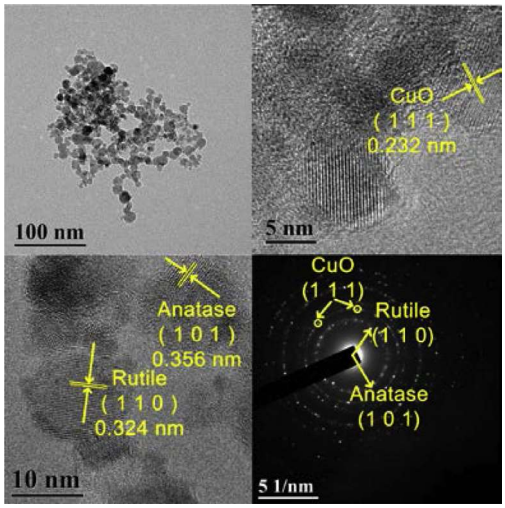

Fig. 3. TEM micrographs and SAED image of the FSP-derived CuO-TiO_2(20CT).

3.2. *CuO-TiO_2 interaction*

XPS analysis is performed to further investigate the surface compositions and elementary oxidation states of these catalysts. Due to the charging effect during XPS analysis, the binding energy scale is calibrated using adventitious carbon (284.6 eV). The XPS spectra of Ti 2p, Cu 2p and O 1 s for Cu-TiO_2 catalysts are displayed in Fig. 4. There are three sets of peaks for Cu 2p, corresponding to Cu $2p_{3/2}$, Cu $2p_{1/2}$ and Cu 2p satellite peak. The peak at 934 eV and the satellite peaks located at 938–946 eV are the characteristics of Cu^{2+} and a peak at 932.9 eV is identified as Cu^{1+} [23]. The binding energy of Cu $2p_{3/2}$ is shown in Table 2. The binding energies of Cu $2p_{3/2}$ for the catalysts are 932.8-934.3 eV, which are slightly higher than those reported for the bulk

Table 2
XPS data for the CuO-TiO_2 catalysts.

Catalysts	Binding energy (eV)		Atomic ratio (%)			Cu^{1+}/Cu	O^{β}/O
	Ti $2p_{3/2}$	Cu $2p_{3/2}$	Cu	Ti	O		
2CT	458.85	932.79	2.39	33.26	64.35	0.65	0.24
8CT	458.48	933.65	9.10	29.38	61.52	0.35	0.32
12CT	458.50	934.29	13.30	27.04	59.66	0.12	0.35
20CT	458.58	933.62	18.77	23.01	58.22	0.33	0.25

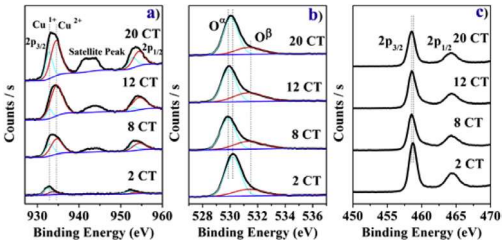

Fig. 4. XPS results profiles of the FSP-derived made CuO-TiO_2. (a) Cu; (b) O; (c) Ti.

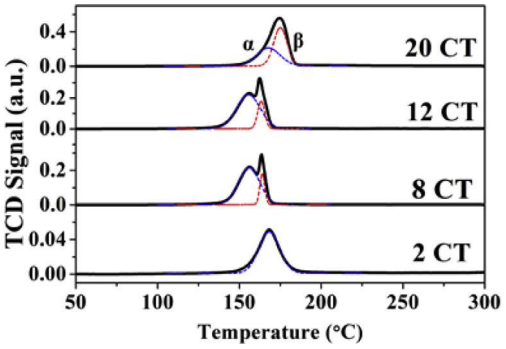

Fig. 5. H_2-TPR profiles of CuO-TiO_2 catalysts.

CuO and Cu_2O materials, indicating a stronger interaction between the metal oxide and the support [24]. Figure. 4b shows the O 1 s XPS spectra of CuO-TiO_2 and the spectra features of the catalysts are numerically fitted. The O 1 s spectra displays binding energy of 530.8 eV for the four catalysts. The O^{α} peak of lower binding energy could be attributed to the lattice oxygen and the O^{β} peak of higher binding energy could be ascribed to the adsorption oxygen species [25]. The adsorbed oxygen is often located near the oxygen defect or vacancy, which confirms the existence of a certain amount of vacancies in the catalysts. The Ti 2p spectra with a binding energy of 455-470 eV are displayed in Fig. 4c. The intensity of Ti 2p peaks decreases with the increase of CuO content, which indicates the decrease of the TiO_2 content on the catalyst surface and the formation of CuO-enriched surface layer. A slight shift of the binding energy of Ti $2p_{3/2}$ is also observed in all the catalysts.

Table 2 shows the simultaneous and opposing changes of Cu $2p_{3/2}$ and Ti $2p_{3/2}$ binding energies. Similar trends are also observed for adsorbed oxygen and Cu^{1+} with the increase of CuO content. With the addition of CuO dopants, the electron transfers to the titanium, which results in the decrease of Cu oxidation state and the increase of titanium and then leading to a strong interaction between CuO and TiO_2. In the FSP process, there are two paths for the formation of Cu_2O. The decomposition of CuO occurs on the surface of the catalyst during the FSP synthesis process. At a high-temperature oxygen-deficiency atmosphere caused by violent combustion of precursor, CuO decomposes into Cu_2O. The other path is the reduction of Cu^{2+} to Cu^{1+} in the strong metal oxide-support interaction ($Ti^{3+} + Cu^{2+} \leftrightarrow Ti^{4+} + Cu^{+}$) [26].

When examining the effects of different CuO loading, we find that 12 wt.% loading of CuO is a turning point among four catalysts. We deduce that the Cu species can no longer embed into the TiO_2 lattice at higher CuO loadings (12 wt.% or higher) [16]. On the one hand, Cu cations concentration in the solid solution cannot increase any more, therefore resulting in a decrease of vacancy concentration and the weakening of the interaction between Cu and Ti. Meanwhile, the number of adsorption oxygen formed near the vacancy would also decrease. The phase transformation from anatase to rutile controlled by the vacancy concentration would also be suppressed. On the other hand, the surplus Cu species would then be deposited on the surface and directly exposed to the high temperature flame to decompose into Cu_2O. With the surface enrichment of Cu species, the particle exceeds a monolayer of surface coverage, thus the amount of discrete CuO or small sized crystallites increases.

As shown in Fig. 5, TPR tests further show the interaction between CuO and TiO_2. Two reduction peaks at 140–190°C were observed which is corresponding to the stepwise reduction of different CuO species. The peak α corresponds to the reduction of finely dispersed particles which are prone to be reduced at low temperatures, and the peak β is assigned to the reduction of relatively larger CuO crystallites species [27].

As shown in Table 3, the area of peak β increases when increasing CuO content, which

Table 3
TPR data measured for CuO-TiO_2 catalysts.

Catalysts	α peak		β peak		H_2 uptake	H_2/Cu
	T(°C)	Area(%)	T(°C)	Area(%)	(mmol/g)	
2CT	168.3	100	–	–	0.33	1.29
8CT	155.6	83.62	164.0	16.38	1.35	1.36
12CT	154.0	80.38	163.4	19.62	1.70	1.14
20CT	167.8	45.01	170.1	54.99	2.81	1.12

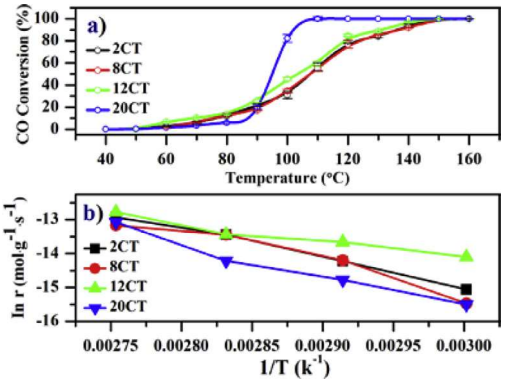

Fig. 6. (a) CO conversion and (b) Arrhenius plots for CO combustion.

indicates the increase of CuO crystallites. When the CuO content is lower than 12 wt.%, the onset temperature of CuO reduction decreases with the increase of CuO content. This may be ascribed to the hydrogen spillover effect: the bulk Cu islands form in the reduction period α, and more CuO leads to easier production of Cu islands, thus making reactions more likely to occur [28]. At a lower CuO loading, the amount of Cu islands controls the reduction rate because that the CuO species exist as small crystallites and is easy to be reduced. At a higher CuO loading of 20 wt.%, crystallites size controls the formation rate of Cu islands due to the growth of small crystallites. The hydrogen uptake of four catalysts is shown in Table 3. All the catalysts prepared by FSP consumed excess hydrogen compared with their CuO content even though there is certain amount of Cu^{1+} in the material. The excess hydrogen consumption is attributed to reduction of Ti^{4+} in the SMSI effect which has been reported in many literatures [29,30]. Evidence of the reduction of TiO_2 can be found from the color of the catalysts, which changes from light green and light brown before reduction to dark black after reduction.

3.3. Catalytic combustion performance evaluation

The catalytic combustion performance of the 1.5 vol.% CO is shown in Fig. 6a. CO begins to be oxidized at 50°C. When the temperature is between 50–90°C, the CO conversion increases slowly. 12CT exhibits the highest CO conversion rate at 40-80°C, indicating 12CT possesses the best catalytic performance at lower temperatures among all the catalysts. This is probably ascribed to its excellent oxidation properties, as confirmed by the TPR experiment.

At temperature of 90–100°C, the CO conversion rate of 20CT increases rapidly and a 90% conversion of CO is achieved at 105°C. There is a sudden change in curvature at T = 85°C for 20CT and we infer that it is related to the type of active sites that play a major role in catalytic reaction at different temperatures. When the temperature is lower than 85°C, the relative smaller CuO species play a major role in the reaction, and that perhaps is the reason why 12CT with a largest amount of discrete CuO species has a better performance at this period. While the temperature is higher than 85°C, the CuO species with relative larger crystallite play the major role in the reaction. The other three catalysts achieve a conversion rate of 90% at 140°C. Compared with CuO-TiO_2 catalysts synthesized by deposition–precipitation method [7], the FSP-synthesized catalysts show better performance on CO catalytic combustion, e.g., a 20°C decrease on 90% conversion temperature. The Arrhenius curve from CO catalytic combustion is shown in Fig. 6b. When calculating the apparent activation energy, a temperature range of 40-80°C is chosen to ensure that the CO conversion is below 20% so that it can be assumed to be a differential reactor at this state [31]. 12CT exhibits the lowest activation energy of 32.50 kJ/mol, which is in consistence with its good catalytic performance at lower temperature. In order to further investigate the performance of the catalysts, the catalyst is tested under different atmospheres. As shown in Table 4, 2CT, 8CT and 12CT demonstrate low conversion at higher CO concentration. This may be attributed to the lack of the active phase on the catalyst surface. Thus, an excessive amount of CO could not be accommodated to react with O_2. On the contrary, 20CT exhibits a decreased conversion when the CO concentration is 1 vol.%, which may be ascribed to lack of intermediate phase in the material during the catalytic reaction. When the concentration of O_2 increases, the conversions of all sample decrease. This may result from the competitive adsorption between O_2 and CO on the catalysts surface.

Table 4
Catalytic data measured for CuO-TiO_2 catalysts.

Catalysts	T_{90} (°C)	T_{50} (°C)	Activation energy (kJ/mol)	CO conversion rate at different reaction conditions (100°C)		
				1%CO + 4% O_2	2%CO + 4% O_2	1.5%CO + 21% O_2
2CT	130 ± 3	105 ± 6	78.46	45% ± 2%	41% ± 1%	40% ± 1%
8CT	130 ± 4	103 ± 5	77.57	48% ± 2%	45% ± 1%	32% ± 1%
12CT	120 ± 2	98 ± 5	32.50	54% ± 1%	50% ± 3%	51% ± 3%
20CT	100 ± 3	92 ± 2	78.68	68% ± 2%	100% ± 1%	85% ± 2%

Although 20CT has a higher activation energy and a relative poor catalytic activity at lower temperature than 12CT, it achieves a higher CO conversion at a temperature range of 90–140°C. In this experiment, the optimum content of CuO is 20 wt.%, while the threshold loading value for other preparation is 4–10 wt.%. Highly-dispersed CuO with a small crystal size plays the key role in CO catalytic combustion [9]. Although 20CT exceeds the turning point of 12 wt.%, the large crystalline CuO with poor catalytic performance does not appear. It is inferred that although the amorphous would transform into discrete crystallites CuO, the crystallite size is not large enough to affect the reactivity of the active phase. Herein, further enhancement of catalytic combustion performance is observed at 20 wt.% of CuO. In addition, the proportion of rutile and anatase is also an important factor affecting the catalytic properties of CO catalytic combustion. Factually, CuO on anatase surface is difficult to be reduced and shows lower catalytic activity for CO oxidation [32]. Therefore, the FSP-made CuO-TiO_2 achieves two pivotal functionalities: (1) increasing the threshold of CuO content, and (2) increasing the rutile content in the catalysts. The joint effect of two functions remarkably promotes the catalytic combustion of CO.

The time-on-stream test is carried out to further investigate the stability of the catalysts. 20CT is tested in the stream of 120°C (1.5 vol% CO, 6 vol% O_2, and 93 vol% N_2, 60,000 mL/(g·h)). As shown in Fig. 7, after 7 hours of reaction, the catalyst still maintains a high CO conversion of about 95%, indicating that the catalyst has excellent stability. The characterization of the catalyst after reaction shows that the long time catalytic combustion reaction does not have a significant influence on the structure of the catalyst, and the CuO crystals are still not found in any catalyst (see **Section S5** of SM for more details). Although some carbonates are formed on the catalyst surface, considering that ethanol is used in this work, it may be difficult to avoid the formation of the carbonates during the synthesis and collection of nanoparticles. According to time-on-stream results, the carbonates is not enough to affect the performance of the catalysts.

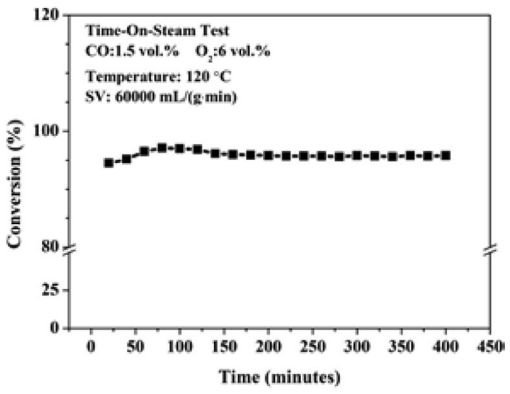

Fig. 7. Time-on-stream test of 20CT.

4. Conclusions

Flame spray pyrolysis is demonstrated to be an effective method for preparing CuO-TiO_2 nanocatalysts for CO catalytic combustion. In this work, the optimum content of CuO for CO catalytic combustion is 20 wt.%, which is evidently higher than that prepared by conventional routes (typically less than 8%). A comprehensive mechanism is proposed for understanding the effects of CuO content on the physicochemical properties of the as-synthesized catalysts and their catalytic combustion performance.

The embedding of copper cations into the TiO_2 lattice changes the crystallite lattice spacing of TiO_2 and promotes the transformation from anatase to rutile due to the presence of the oxygen vacancies. The formation of oxygen vacancies caused by the addition of dopant Cu^{2+} results in an enhanced diffusion of oxygen ions. As a result, the TiO_2 sintering rate controlled by the diffusion of oxygen ions will increase.

12 wt.% loading of CuO is the turning point of physical-chemical properties of the as-prepared catalysts. Cu species cannot any longer embed into the TiO_2 lattice at a higher CuO loading than 12 wt.%. Cu cations concentration can no longer increases in the TiO_2, the interaction between Cu and Ti is weakened and the vacancies in the catalysts decrease. The enrichment of Cu species on the surface results in an increasing content of Cu^{1+}, and thus the amount of larger crystallite increases.

The FSP method is demonstrated to be effective for improving the performance of catalysts by improving the CuO content and the ratio of stable rutile phase. Even at the highest CuO content of 20 wt.%, there is no large CuO crystallite on the catalyst surface which achieves a considerable amount of highly active phase and therefore promotes the reaction performance. A high rutile content can avoid the strong interaction between CuO and TiO_2, as thus the high catalytic activity is obtained.

Acknowledgments

This work was founded by "National Natural Science Foundation of China (51522603 and 51606079)".

Supplementary materials

Supplementary material associated with this article can be found, in the online version, at doi:10.1016/j.proci.2018.05.102.

Appendix A. Supplementary material

Supplementary material associated with this article can be found, in the online version, at http://ees.elsevier.com/proci/.

References

[1] A. Elmhamdi, L. Pascual, K. Nahdi, A. Martínez-Arias, *Appl. Catal. B* 217 (2017) 1–11.
[2] B. Kucharczyk, W. Tylus, J. Okal, J. Chęcmanowski, B. Szczygieł, *Chem. Eng. J.* 309 (2016) 288–297.
[3] S. Royer, D. Duprez, *Chem. Cat. Chem.* 3 (2011) 24–65.
[4] C. Galeano, R. Güttel, M. Paul, P. Arnal, A.H. Lu, F. Schüth, *Chem. Eur. J.* 17 (2011) 8434–8439.
[5] D. Widmann, R.J. Behm, *Acc. Chem. Res.* 47 (2014) 740–749.
[6] M.Y. Kang, H.J. Yun, S. Yu, W. Kim, N.D. Kim, J. Yi, *J. Mol. Catal. A: Chem.* 368-369 (2013) 72–77.
[7] H. Li, J. Zhou, B. Feng, *J. Porous Mater.* (2016) 1–6.
[8] A.L. Luna, M.A. Valenzuela, C. Colbeau-Justin, et al., *Appl. Catal. A* 521 (2016) 140–148.
[9] H. Chen, H. Zhu, Y. Wu, F. Gao, D. Lin, J. Zhu, *J. Mol. Catal. A: Chem.* 255 (2006) 254–259.
[10] B. Xu, L. Dong, Y. Chen, *J. Chem. Soc, Faraday Trans.* 94 (1998) 1905–1909.
[11] S. Li, Y. Ren, P. Biswas, S.D. Tse, *Prog. Energy Combust. Sci.* 55 (2016) 1–59.
[12] Y. Zong, S. Li, F. Niu, Q. Yao, *Proc. Combust. Inst.* 35 (2015) 2249–2257.
[13] N. Wang, S. Li, Y. Zong, Q. Yao, Y. Zhang, *Proc. Combust. Inst.* 36 (2016) 1029–1036.
[14] F.E. Kruis, H. Fissan, A. Peled, *J. Aerosol Sci.* 29 (1998) 511–535.
[15] M.S.P. Francisco, V.R. Mastelaro, *Chem. Mater.* 14 (2002) 2514–2518.
[16] R. Kydd, W.Y. Teoh, K. Wong, et al., *Adv. Funct. Mater* 19 (2009) 369–377.
[17] S. Tangsir, L.D. Hafshejani, A. Lähde, et al., *Chem. Eng. J.* 288 (2016) 198–206.
[18] V. Srinivas, S.E. Pratsinis, *J. Am. Ceram. Soc.* 78 (2010) 2984–2992.
[19] D.A.H. Hanaor, C.C. Sorrell, *J. Mater. Sci.* 46 (2011) 855–874.
[20] R.D. Shannon, J.A. Pask, *J. Am. Ceram. Soc.* 48 (1965) 391–398.
[21] C. Chaisuk, A. Wehatoranawee, S. Preampiyawat, S. Netiphat, A. Shotipruk, *Ceram. Int.* 37 (2011) 1459–1463.
[22] P.S. Barbato, S. Colussi, A.D. Benedetto, et al., *J. Phys. Chem. C* 120 (2016).
[23] X. Yao, L. Zhang, L. Li, et al., *Appl. Catal.* 150-151 (2014) 315–329.
[24] Y. Zeng, T. Wang, S. Zhang, Y. Wang, Q. Zhong, *Appl. Surf. Sci.* 411 (2017) 227–234.
[25] M. Konsolakis, Z. Ioakeimidis, *Appl. Surf. Sci.* 320 (2014) 244–255.
[26] C. Deng, B. Li, L. Dong, et al., *Phys. Chem. Chem. Phys.* 17 (2015) 16092.
[27] M.Y. Kang, W. Kim, B.J. Ji, N.D. Kim, H.J. Yun, J. Yi, *Catal. Lett.* 132 (2009) 417–421.
[28] N.W. Hurst, S.J. Gentry, A. Jones, B.D. McNicol, *Catal. Rev.* 24 (1982) 233–309.
[29] H. Zhu, Z. Qin, W. Shan, W. Shen, J. Wang, *J. Catal.* 225 (2004) 267–277.
[30] Y. Li, B. Xu, Y. Fan, et al., *J. Mol. Catal. A: Chem.* 216 (2004) 107–114.
[31] W. Han, G. Zhang, G. Lu, Z. Tang, *RSC Adv.* 5 (2015) 59666–59676.
[32] H. Zhu, Y. Wu, X. Zhao, *J. Mol. Catal. A: Chem.* 243 (2006) 24–30.